UC Berkeley
UC Berkeley Previously Published Works

Title

Metal—Organic Frameworks: Challenges Addressed via Magnetic Resonance Spectroscopy

Permalink

https://escholarship.org/uc/item/4zh2823v

Journal

Applied Magnetic Resonance, 54(11-12)

ISSN

0937-9347

Authors

Funke, Lena Marie
Lund, Alicia
Zhuang, Hao
et al.

Publication Date

2023-12-01

DOI

10.1007/s00723-023-01604-0

Peer reviewed

eScholarship.org Powered by the California Digital Library
University of California

Applied Magnetic Resonance (2023) 54:1193–1220
https://doi.org/10.1007/s00723-023-01604-0

Applied
Magnetic Resonance

REVIEW

Metal–Organic Frameworks: Challenges Addressed via Magnetic Resonance Spectroscopy

Lena Marie Funke[1] · Alicia Lund[1] · Hao Zhuang[1] · Jeffrey A. Reimer[1]

Received: 21 June 2023 / Revised: 10 August 2023 / Accepted: 17 August 2023 /
Published online: 5 October 2023
© The Author(s) 2023

Abstract

Magnetic resonance spectroscopies occupy a premier position within the chemical sciences by revealing structure and dynamics in molecules and solids associated with photosynthesis, enzymology, Alzheimer proteins, pharmaceuticals, catalysts, polymers, and electronic materials. Here, we review the recent literature contributions of NMR and EPR spectroscopy towards the study of metal–organic frameworks from 2017 to mid-2022. We organize the review around what we perceive to be the intellectual challenges in MOF research: structure, dynamics, synthesis, properties, and function.

1 Introduction

Metal–organic frameworks [1] provide for a near infinite number of metal–ligand combinations and, thus, exhibit a rich diversity of structures, chemistries, and topologies. This diversity is paired with an exquisite level of synthetic and geometrical control of structure due to the modular nature of framework synthesis, allowing for the consistent production of near-ideal pore structures whose key parameters, such as pore size or pore chemistry, may be tuned independently [2]. These breakthroughs in chemical diversity, control, and reproducibility of MOFs contrast with the inherent chemical limitations of traditional microporous materials such as porous carbons, silicas, and zeolites. As a result, fundamental research studies of MOFs have flourished, as have industrial applications. For example, MOFs possess inherently tunable modular structures, and this tunability has led to novel materials exhibiting record-breaking porosities and specific surface areas [3]. Virtually every gas [4] and liquid [5] separation process, as well catalytic and photocatalytic chemistries [6],

✉ Jeffrey A. Reimer
reimer@berkeley.edu

[1] Department of Chemical and Biomolecular Engineering, Materials Science Division, Lawrence Berkeley National Laboratory, UC Berkeley, University of California, Berkeley 94720, USA

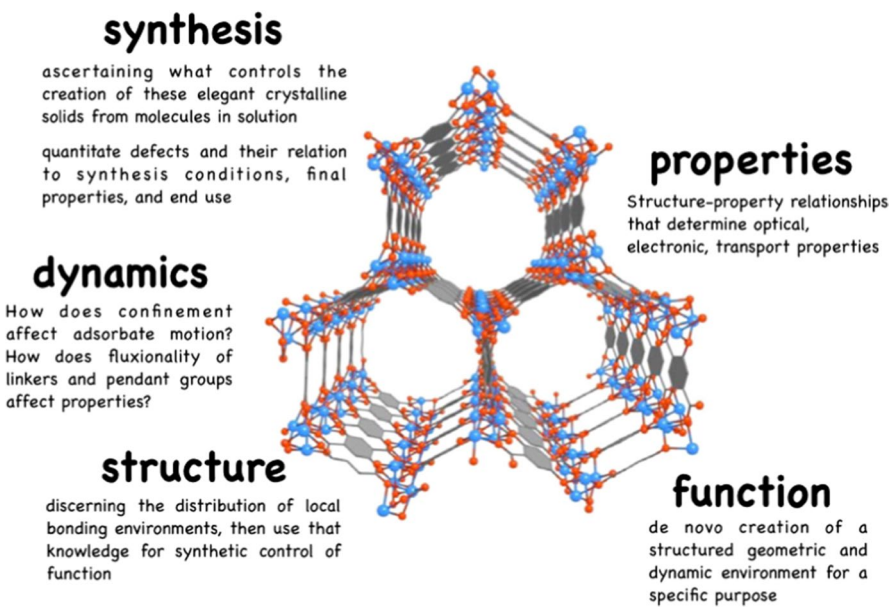

Fig. 1 In black are the grand challenges for emerging research in metal–organic frameworks

are being addressed by MOF researchers. According to the Web of Science between 2017 and mid-year 2022 alone, there were 6011 review articles written on MOFs.

Several grand challenges remain, however, in understanding these compelling materials (Fig. 1). Among the most important, we identify: discerning the distribution of local bonding environments, then using that knowledge for synthetic control of function [7]; ascertaining what controls the creation of these elegant crystalline solids from molecules in solution [8]; measuring how confinement directs the transport of liquids and gases [9]; development of new metrologies for interactions between walls and adsorbates to inform theory and simulation [10]; de novo creation of a structured geometric and dynamic environment for a specific purpose [11]; development of analytical methods that span multiple length and time scales [12]; and quantitation of defects and their relation to synthesis conditions, final properties, and end use [13]. Each of these grand challenges poses technical hurdles for analytical and structure determination methods. The goal of this brief review is to present how solid-state and related MR methods are being used to address these challenges. We conclude by speculating on future challenges in MOF research and how some of them can be addressed by MR.

In sharing NMR reviews with non-NMR colleagues, the question often arises as to why researchers should choose magnetic resonance methods at all, given that the method is notoriously insensitive and requires highly specialized instrumentation and expertise. We urge our colleagues to affirm that NMR is characterized (and differentiated) by two critical attributes [14]: first, very long lifetimes of the nuclear spin quantum states that afford extensive experimental manipulation of spins to reveal specified NMR properties (shifts, couplings); second, the "phase" of the radio

waves applied to, and emanating from, nuclear spins are measured experimentally using quadrature detection thereby affording temporally selected quantum coherence transfer pathways that minimize artifacts and present spectra of quadrupolar nuclei with the resolution of liquids NMR. These two attributes are essential to applications of NMR to MOFs, for example by yielding quantitation of useful observables, e.g., the chemical shift of an atom on the MOF linker and its proportion relative to other atoms.

2 Challenge #1: Structure

Here, we focus on the issues associated with chemical structure (e.g., who is bonded to whom) presented in the literature between 2017 and mid-2022. Common in this era is the routine use of NMR spectroscopy to probe local bonding environments within MOF crystals with mixed metals [15, 16] or mixed linkers [17–20]. We focus below on *hybrids and glasses* made from MOFs because they are difficult to probe with alternative methods such as crystallography and microscopy. More specifically, we review NMR methods that resolve distributions of local bonding environments in and between domains, with the intent for synthetic control of material function.

2.1 MOF Glasses

The motives for developing glass MOFs are clear: upscaled MOF syntheses usually yield crystalline MOF powders that pose several challenges in application. First, loosely packed powders quench gas adsorption capacity by, e.g., 35% for methane in HKUST-1 [21] Second, MOF powders compact with exposure to pressurized gas over time, thereby causing pressure drop in adsorption columns and dust formation—vexing problems in application that complicate transport and recycling. Finally, the void space between crystallites represents unused space, an anathema to practical application. Although void spaces may be customized in hybrid materials [22–25] with moieties other than the linkers and, thus, present potential synergisms such as pathways for molecular and heat transport [26], the voids can be eliminated completely in MOF glasses. These MOF glasses are melt-cast into different shapes to yield properties beyond their crystalline counterparts. Initial NMR results on MOF glasses and the progress in hybrid materials are, thus, emerging as a promising area of study.

While glass types such as oxidic, metallic, and polymeric glasses are well known, in 2015 MOF glasses [27–31] were discovered. Researchers have since synthesized MOF glasses via several different pathways so as to explore their properties. As some MOF glasses are chemically variable and can feature permanently accessible pores [32], their amorphous state offers the unprecedented combinations of material properties within characteristic MOF chemical landscapes.

All glasses lack a long-range order and, thus, their properties depend on ordering effects, best described by distributions functions of atom positions, distances, and angles. These distributions are not easily characterized with methods

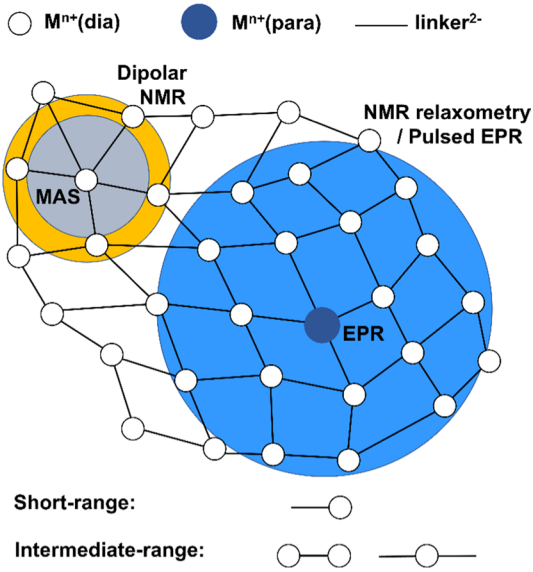

Fig. 2 Length scale of short- and intermediate-range order in a MOF glass and magnetic resonance methods: MAS NMR (gray), Dipolar NMR (yellow), EPR (dark blue), and NMR relaxometry/Pulsed EPR (light blue). Derived from Fig. 16 in https://doi.org/10.1111/ijag.12333

standardly employed for MOF crystals. As illustrated in Fig. 2, NMR and EPR spectroscopy probe these distributions on different length scales: chemical shifts, dipolar-determined distances, EPR hyperfine structure and DEER distances, and relaxometry. These methods discern short-, intermediate-, and medium-range distances representing the first, second, and third coordination sphere around linkers or metal nodes. Initial recent research on MOF glasses provides insights on those three lengths scales, as discussed below.

2.1.1 Short-Range Order

ZIF-62 of composition $[Zn(Im_{2-x}bIm_x)]$ with imidazolate (Im) and benzimidazolate (bIm) linkers forms glasses comprised of $Zn[ligand]_4$ tetrahedra. To improve optical properties towards use in photonics, researchers ponder what controls the connectivity of the tetrahedra in ZIF-62 glasses. Clearly, ^{67}Zn NMR is sensitive to small changes in the coordination sphere of Zn (^{67}Zn = spin-5/2) since the electric field gradient at the Zn^{2+} atom alters in magnitude and symmetry with changing coordination. Vitrified ZIF-62 exhibits ^{67}Zn NMR spectra that show how the distribution of C_Q, δ_{iso}, and η_Q parameters reflects the distribution of Zn–N distances and N–Zn–N angles [33]. Modifying the structure by, e.g., halogenating linkers in ZIF-CU-4 glass, increases the gas-adsorption capacity [34], yet the ^{19}F NMR spectra in these glasses display broad resonances at around − 220 ppm reflecting direct Zn–F bonds that vitrification scrambled local fluorine bonding. In spite of these bonding changes, the glass MOFs show impressive adsorption capacities [35].

2.1.2 Intermediate- and Medium-Range Order

ZIF-62 glass can also accommodate MIL-53 crystals that remain in their high-temperature, open-pore phase at room temperature, thus making ZIF-62 an interesting glass host matrix for crystalline MOFs [26]. The amorphous and crystalline phases of these mixed composite materials were characterized [32] via ^{1}H MAS, ^{13}C CP MAS, ^{1}H-^{1}H, and ^{13}C–^{1}H spin-diffusion experiments, where researchers assigned the ^{13}C NMR resonances of the linker molecules with Lee–Goldberg CP experiments. In the ZIF-62 glass, the ^{13}C-detected spin-diffusion NMR experiment demonstrates that the inter-linker distances between the two types of linkers, 5-methylbenzimidazolate and imidazolate, decrease with vitrification, while porosity stays intact. Medium-range order in this mixed composite glass-crystal MOF system was probed via ^{1}H spin-diffusion curves; here, the authors emphasized the sub-nano proximity of imidazole linkers in ZIF-62 and the OH groups of MIL-53. As those functional groups belong to different domains inside the material, these results detail the phase boundaries between materials, showing that the active functional groups of the two composites achieve sub-nanometer proximity. This single reference perhaps best represents the opportunities for structure determination in MOF glass and composites.

There is an ever-growing MOF library of synthesized MOFs that presents > 20,000 structures, offering a great variety of chemistries to pick from and generate new libraries for MOF composites and glasses. It is anticipated that a host of new applications will emerge from these libraries. As illustrated by the research between 2017 and mid-2022, magnetic resonance spectroscopy assists this exploration by examining the intermingling of local bonding configurations at length scales difficult to measure with other methods.

2.2 Polymer–MOF Hybrid Materials

Polymer–MOF *hybrid materials* find applications in, e.g., CO_2 adsorption and conversion, 24 and protective wearables [22–25]. To determine which polymers in a membrane infiltrate the pores or coat the surfaces of UiO-66 crystals, ^{1}H–^{13}C spin-diffusion NMR has been gainfully employed. Here, the researchers measured the ^{13}C–^{1}H spin-diffusion NMR build-up curves of the polymer –CH_2 and benzene–H protons in UiO-66 as a function of spin-exchange time [36]. Figure 3 shows the experimental and theoretical build-up curves for polyethylene oxide (PEO) with a model that assumes PEO interpenetrates the UiO-66 crystals. The steep build-up can only be explained by efficient spin-diffusion between the CH_2 (polymer) and H (MOF). This fast build-up confirms that the spin-diffusion transport distance is small and matches the theoretical model for PEO infiltrating the MOF pores. In contrast, polyvinylidene fluoride (PVDF) coats the surfaces of UiO-66 as illustrated by the flat spin-diffusion build-up.

Other researchers studied polymers reacting with functional groups on MOF UiO-66 via ^{13}C solids NMR spectroscopy [20]. The researchers dispersed UiO-66-NH_2

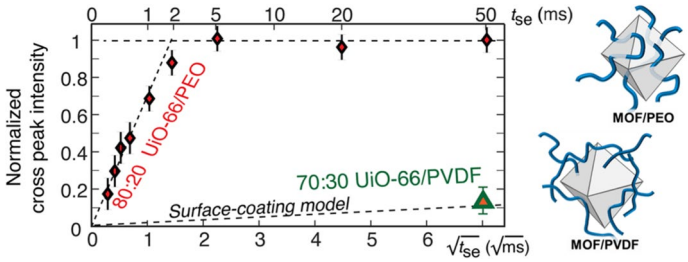

Fig. 3 Spin-diffusion ^{13}C–^{1}H build-up experimental (dots) and molecular dynamic simulation (lines); here t_{se} represents the mixing time for exchange. PVDF coats the surface of UiO-66; PEO interpenetrates the crystals as apparent by the build-up curves. [36] Adapted from Reference

particles into the monomer mix during polymerization of PIM-1. This polymer was found to deposit on the surface of UiO-66 as the ^{13}C solids NMR spectrum reveal three distinct ^{13}C resonances in between 30 and 60 ppm. With the polymerization reaction progressing, the ^{13}C NMR resonance assigned to amine-linked carbon at 150.9 ppm shifts to 161 ppm, confirming primary amines transform into secondary amines during PIM-1 and UiO-66-NH_2 cross-linking.

3 Challenge #2: MOF Synthesis

MR spectroscopy can inform the MOF designer about the parameters that control MOF nucleation and crystal growth, particularly with respect to ascertaining what controls the creation of MOFs from molecules in solution, as well as quantitate defects and their relation to synthesis conditions, final properties, and end use.

3.1 Crystal Growth and Defects

Because NMR can easily discern liquid and solid states, it can probe the evolution of crystal components from reacting precursors. For example, the evolution of MFM-500(Ni) from solution [37], from stages of clustering to the formation of crystals, was examined using ^{1}H NMR. From the plot of the ^{1}H signal intensity as a function of time, activation energies for nucleation and crystallization of MFM-500(Ni) were obtained. In addition to ^{1}H NMR, direct excitation and cross-polarization ^{13}C NMR can differentiate species in solid phase and liquid phase. Here, authors combined time-resolved ^{27}Al and ^{13}C direct excitation with ^{1}H–> ^{13}C cross-polarization to understand the mechanism of MIL-53(Al) crystallization by tracking the concentration of different species in both phases. We surmise that custom-built probes and bench top instruments will likely extend this genre of study to more elaborate synthesis conditions. We note that even though PFG NMR is well-suited to study diffusion in multicomponent systems, self-diffusion during early stages of synthesis of key molecules during MOF formation still needs to be studied more intensively.

Non-conventional synthesis techniques can yield new MOF topologies, as demonstrated [38] in a solvent-free accelerated aging synthesis route for $Cd(MeIm)_2$.

These accelerated-aging syntheses yield a topology with a Cd: MeIm ratio of 1:3 according to solid-state NMR, but 1:2 according to X-ray diffraction. To test the hypothesis of a new dia-topology and to study the progression of the Cd coordination, the authors deploy ^{111}Cd, ^{13}C, and ^{14}N NMR. This NMR-enhanced crystallography applied to the $Cd(MeIm)_2$ MOF family may help to explore new synthesis pathways of MOFs beyond $Cd(MeIm)_2$. We envision crystallization studies of MOFs to profit when expanded to other isotopes as ^{31}P, and ^{19}F NMR, possibly $^{35/37}$Cl and $^{79/81}$Br NMR [39] and DNP- NMR.

Negative gas adsorption (NGA) occurs when MOF structural contraction triggers gas expulsion, and it has important implications for gas separation and energy storage applications [40]. An example of NGA comes from the MOF DUT-49 that undergoes negative gas adsorption at a threshold pressure with a step-shaped isotherm where the position and shape slightly change with the crystal size. To discern if this effect originates from the higher concentration of (1) surface or (2) defect sites with decreasing in crystal size, the authors [41] compared the adsorption isotherms and ^{129}Xe NMR spectra for a concentration and defect series of DUT-49 samples. They report ^{129}Xe chemical shifts decreasing with crystal size, thereby can assign the larger surface to volume ratio—not the defect concentration—as the origin of the change in adsorption behavior.

3.2 Functionalization/Pore Formation

Integration of functional groups post-synthetically into MOFs is a promising strategy to tailor functionality. Here, solid-state NMR has been used to analyze the relation of functional groups and conditions for their integration [34]. For example, a hierarchically porous MOF is formed by heat-triggered decarboxylation [42] of the linkers in microporous MIL-121 (an aluminum based MOF), yielding anhydride functional groups that are easily appended with differing chemical functional groups, or even Pt-metal atoms. Different annealing conditions, such as the temperature and duration of annealing, lead to covalent biding of, e.g., ten differing chemical functionalities at the anhydride positions that exhibit enhanced gas adsorption of CO_2, C_2H_2, C_2H_4, and CH_4. Here, the effect of different thermal activation conditions on the mobility, the number, and the relative host–guest interaction strengths of different gas molecules has been studied with static VT NMR. The mechanism responsible for decarboxylation was studied with ^{27}Al MAS, ^{13}C CP MAS, and ^{1}H MAS NMR spectroscopy. The authors report that as a fraction of the carboxylate linkers converts to anhydride, Al(V) is partially converted to open Al(V) coordination environments, resulting in increased pore sizes. The anhydrides can also serve as anchors to introduce Pt complexes that were shown to be effective for electrocatalytic reactions.

3.3 Fast Screening

Given that MOFs represent libraries of compounds that are theoretically on the order of millions of structures, researchers demand fast screening methods to assess material properties in cooperation with variations in synthesis methods. One effective

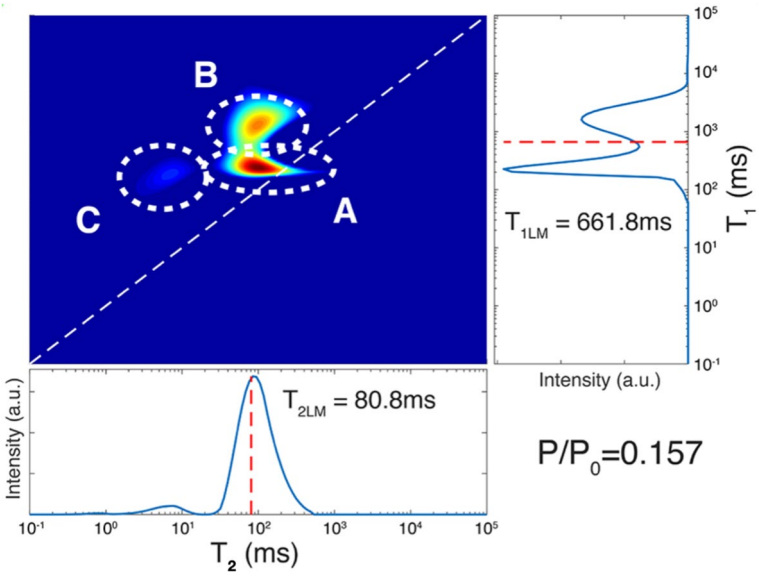

Fig. 4 2D relaxometry, in the form of a $T_1 - T_2$ correlation map, presents three adsorbate populations for MeOH loaded into ZIF-8 (from Reference [43])

strategy for screening materials is discernment of surface area or pore volume, yet volumetric methods for doing so are frustratingly slow. Researchers recently acquired adsorption isotherms by quantifying NMR peaks intensities and measuring relaxation rates (R_1 and R_2) of adsorbed gas molecules in low-field benchtop instruments [43]. They were able to rapidly measure a number of adsorbates as a function of partial pressure, in contrast to very slow sorption analyzers. These (and other authors) have shown that low-field NMR relaxometry is characterized by results similar to those from sorption analyzer isotherms, have modest purchase and maintenance costs, are non-destructive (yet requires 20 mg of sample), provide chemical adsorption site resolution, and (importantly) are applicable to gases and gas mixtures. In reference 43 the authors report that as the R_1 and R_2 of gas molecules differ according to the adsorption sites specifics—including host–guest interactions, guest–guest interactions, quantity and type of defects—different sites can be resolved. The researchers conclude that methanol in ZIF-8 adsorbs at cage windows, defect sites, and in clusters in the pore center. Each of the sites has a characteristic R_1, R_2 combination (fingerprint) and R_1, R_2-resolved 2D experiments reflect type and population that can be recorded at any point in the adsorption isotherm (Fig. 4). The researchers also resolved ethanol entering into the tetrahedral and octahedral pores in UiO-66(Zr) sequentially as the sites differ in their R_2 relaxation. It is worth noting that inverse Laplace methods for analyzing relaxation data provides a powerful tool for 1D and 2D relaxometry.

Low-field methods may be selective to adsorbed molecules on pore walls, as opposed to molecules in the pore space owing to the dramatic differences in density. That is, signal emanating from the many adsorbed molecules on pore walls might

vastly exceed the signal from the vastly fewer molecules associated with pore spaces, resulting in NMR yielding an underestimation of isotherms. For example, in the case of very strong wall adsorption of EtOH in ZIF-8, the low-field NMR adsorption isotherms for the pure gases underestimate adsorption as reflected by comparison to traditional measurements at low partial pressures. Moreover, the strong wall–alcohol interactions at low pressures increase local spin density so as to accelerate transverse (R_2) relaxation rates, resulting in partial (unintended) loss of signal intensity.

Low-field NMR relaxometry may be used in cases where adsorption isotherms are difficult to obtain. Water adsorption isotherms, for example, usually require a long time to acquire, are limited to MOFs stable in water, and stress researchers owing to long equilibration timescales and competitive adsorption of water by the tubing connecting elements of the apparatus. Relaxation time-resolved low-field NMR may facilitate studies of water–MOF interactions, as demonstrated by recent hydrophilicity studies [44]. As relaxation times are sensitive to changes of host–guest interactions, guest–guest interaction, and phase changes, we envision a large range of MOFs suitable for low-field adsorption studies, including defective and flexible MOFs.

4 Challenge #3: Dynamics

Running "molecular machines" and "molecular factories" in MOFs is an alluring concept [45]. Being able to modulate motions in operando within a MOF encompasses operational triggers such as light, pH, and temperature, all of which are amenable MOF structural design. Researchers have studied molecular dynamics in MOFs, and in particular the dynamics of linkers with limited flexibility due to coordination in the framework and guest molecule motion in confinement of the pores. NMR spectroscopy takes a detective role in elucidating subsequent structure–dynamic–property relations and below we review new insights NMR spectroscopy provides for final MOF performance.

4.1 Dynamics of Guest Molecules

Molecules that diffuse rapidly in pores (CO_2, H_2O, hydrocarbons) reduce the costs and sizes of adsorption columns and membranes for separation owing to minimal transport limitations and quick cycling times in unit operation processes.[1] Pulsed-field-gradient NMR spectroscopy has the advantage of quantifying self-diffusion coefficients under conditions relevant for technological applications. For example, researchers have studied the influence of multiple guests [46, 47] and toxins, including H_2S, on the diffusion properties in MOFs using PFG NMR. Water mobility was

[1] A word of caution, however. Transport within a MOF may not be the deciding factor in unit operations: the transport of relevant gases (or liquids) in the final construct used in the unit may be most important. For example, a polymer–MOF hybrid may exhibit gas transport limitations because the polymer, or polymer–MOF interface, is transport limiting.

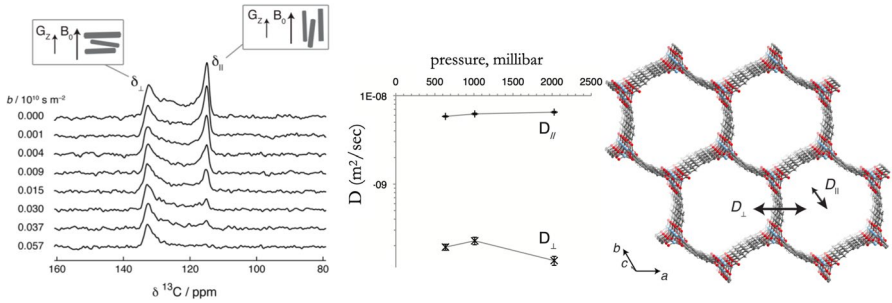

Fig. 5 Residual chemical shift anisotropy of long-range diffusing $^{13}CO_2$ was used to measure magnitude and directionality of diffusion. Left: the change in the CO_2 NMR signal as a function of shift (crystallite orientation) and gradient strength b. Middle, the magnitude of self-diffusion along and perpendicular to the channel. Right: visualization for the pore channel in MOF-275 [50]

studied in hydrophobic ZIF-8 capped with a conducting hydrophilic polymer [48] to inform design the diffusion pathways of water to and around MOFs. The increased water mobility around the MOF suggests the polymer surfaces can transport ions dissolved in water to a hydrophobic MOF.

4.1.1 Long-Range Diffusion

In M_2(dobdc) (M = Mg, Ni, Zn; dobdc^{4-} = 2,5-dioxido-1,4-benzenedicarboxylate, a.k.a. MOF-74), the self-diffusion of CH_4—according to longitudinal relaxation rates R_1—is inversely related to the metal–CH_4 binding energy [49]. These authors further found that the CH_4–CH_4 interactions lower the energy barrier for translational gas diffusion in between metal sites along the *c*-axis. However, at elevated pressures, self-diffusion decreases as CH_4–CH_4 collisions increase.

The residual chemical shift anisotropy of long-range diffusing $^{13}CO_2$ in Zn_2(dobpdc, MOF-274) provided an interesting measurement of the magnitude and directionality of CO_2 self-diffusion rates at high accuracy [50]. Using 750 μm × 120 μm single crystals, the researchers measured self-diffusion coefficients along the different crystalline axes under the conditions where root-mean square displacements (RMSDs) of CO_2 are smaller than the crystal size. They observed a non-zero diffusion rate through the walls of the hexagonal pores, a puzzling observation that was attributed to diffusion across framework channels at wall defects (Fig. 5). Further work [51] of the researchers shows the influence of pore size and concentration of defects on the self-diffusion coefficients along and across the framework channels showing higher concentration of defects increases "through-wall" diffusion. Anisotropic diffusion points out crystal engineering as a tool to define diffusion properties of adsorbents and membranes for gas separation and also it is a measure of defects from a functional perspective. These measurements benefit from larger particles where the exchange with CO_2 outside the pores is negligible.

Other studies [52–54] have used the residual chemical shift anisotropy of ^{13}C in CO_2 to reveal the wobbling and hopping motions of CO_2 molecules. The well-known

two-site exchange models discerned diamine mobility in different diamine-appended Mg_2(dobdc) MOFs using variable-temperature ^{15}N MAS NMR [55].

4.1.2 Diffusion In and Out of the Pore

Researchers from Europe and the UK used selective inversion recovery of ^{129}Xe in MIL-53(Al) to determine R_1, thereby yielding Xe atom exchange rates between MIL-53(Al) crystals of two types: those with open pores and those with closed pores. These results, and in particular exchange (EXSY) methods, discern that rate at which xenon atoms move between open and closed forms to be $43 \pm 6\ s^{-1}$ at room temperature [56].

MIL-121 and MOF-74 were studied [57] by NMR for their ion-conducting properties. Two protons from each tetracarboxylate linkers in MIL-121 are ion-exchanged with a $\{Li^+,Na^+\}$ mixture, yielding high Li^+ and Na^+ ion-mobilities. To understand the origin of the high alkali ion conductivities, the authors employed ^7Li, and ^{23}Na NMR relaxometry to report activation energies for the hopping motion. Using ^1H NMR they identified the alkali ion is the main charge carrier, not protons, and observed a Ngai-coupling model for ion motion.

The performance of fuel cells depend on a high H^+ conductivity for charge transfer. A new class of urea-appended MOF-74 offers super-protonic conductivities of $> 10^{-2}$ S cm^{-1}, though the mechanism has previously been unclear [58]. Using ^2H NMR lineshape analyses and relaxometry, the researchers identified immobile protons and protons with motion activated at room temperature. Their results illustrate that transport between urea and water is negligible. Although urea does not function as a direct proton acceptor, urea takes up pore volume hence brings guest H_2O molecules in closer proximity, affording improved proton transport. Further, the urea $–NH_2$ groups exhibit strong hydrogen bonds to H_2O that strengthen association between guest H_2O molecules, also facilitating proton diffusion.

We project future diffusion studies will benefit the study of diffusion phenomena in monoliths, and membranes with micro-particles in the future. Moreover, the self-diffusion of molecules in gas mixtures subject to confined spaces is an open theoretical and experimental topic.

4.2 Dynamic Linkers

As some functionality in living cells relies on molecules to flex, fold, twist, and jiggle, functionality in MOFs relies on linkers and pendant groups to rotate, twist, pirouette, and shuttle. Table 1 correlates properties with motions as determined by NMR spectroscopy—one of the few methodologies that "visualize" those motions.

The NMR spectroscopist tunes the experiment so as to be sensitive to the types and timescales on which motions occur (see Table 1) by choice of: magnetic field, isotope, and pulse sequence. Many studies use temperature-dependent ^2H NMR spectroscopy to discern dynamics. The residual quadrupolar coupling of ^2H, e.g., in an axial environment of a $C–^2H$ bond, reveals the type and velocity of the motion. For example, fluxing linkers and pendant groups react to stimuli including chemical modifications

Table 1 Types of dynamics in MOFs and properties they influence

Type of motion	MOF/citation	Impact on properties	Method
Methyl rotation	MFM-305 [80]	CO_2 adsorption	^{2}H NMR $T_1(T)^a$
1.4×10^6 Hz Phenyl 180°flips	MFM-160 [81]	C_2H_2:CO_2 separation selectivity	^{2}H NMR
Phenyl 180° flips	UiO-66(Zr) [61, 64, 3, 4]	H_2:CH_4 separation selectivity [61]	^{2}H NMR
Phenyl 180° flips	PIZOF [87]	N/A	^{13}C CP MAS NMR, ^{2}H NMR
Phenyl 180° flips	F_2MOF [83]	N/A	^{2}H NMR
Bipy 180° flips, bicyclopentane 10^7 Hz regime	FTR-P1 [84]	N/A	^{2}H NMR, ^{1}H relaxation NMR
2,6-ndc phenyl linkers do not rotate	DUT-8(Ni) [16]	Ergo cooperative framework constituents' reorientation is guest-triggered [16]	2D EXSY ^{2}H NMR
Librations, large-amplitude twists	ZIF-8 [22]	C_3H_6:C_3H_8 separation selectivity	Simulated lattice, dielectric, ^{2}H NMR T_1 and T_2
Bicyclo[2.2.2]octane ultrafast rotation 4.7×10^{10} Hz	$Zn_2(BODCA)_2$ [85]	N/A	^{1}H NMR $T_1(T)^a$, and ^{2}H NMR
F_2-BODCA rotation	$Zn_2(F_2\text{-BODCA})_2$(dabco) [86]	Correlated rotation, rotor–rotor and rotor–lattice interactions	^{19}F NMR T_1(T) and FWHM(T)
~10^{10} Hz librations	UiO-66(Zr) [65]	N/A	^{2}H NMR anisotropy of $T_1(T)^a$
Cooperative Phenyl rotations 0–10^8 Hz	MIL-53 [62] Carboxylate	Gas adsorption, kinetics of guest release	^{2}H NMR
Cooperative Phenyl rotations 0–10^8 Hz	MIL-53-X(X = H, CH_3,NO_2,OH) [87]	N/A	^{13}C–^{1}H dipolar chemical shift correlation (DIPSHIFT) separated-local-field (SLF) NMR
Mechanically interlocked ring molecules (rotaxanes) on linkers pirouette	UWDM-1 [88], UWDM-2 [88], α-UWDM-3 [88], β-UWDM-3 [88], UWDM-5 [88], α-UWDM-6 [89], α-UWDM-7 [89], UWDM-14 [93]	N/A	^{2}H NMR
Mechanically interlocked ring molecules (rotaxanes) on linkers shuttle	UWCM-8 [90], UWCM-9 [90], UWCM-11 [64]	N/A	^{13}C CP MAS NMR

Table 1 (continued)

Type of motion	MOF/citation	Impact on properties	Method
Rotation of 2,3-difluorophenylene	PIZOF-2F [91]	N/A	^{13}C CP MAS NMR
Torsional flipping of 4,4'-bipyridine	ELM-11 [92]	N/A	^{1}H NMR $T_1(T)^a$, $T_2(T)^b$, and $T_{1\rho}(T)^c$
Rotation of interlocked olefin threads	UMUMOF-3 [94]	N/A	^{2}H NMR

[a] $T_1(T)$: Longitudinal relaxation time as a function of temperature

[b] $T_2(T)$: Transversal relaxation time as a function of temperature

[c] $T_{1\rho}(T)$: Longitudinal relaxation time constant in the rotating frame

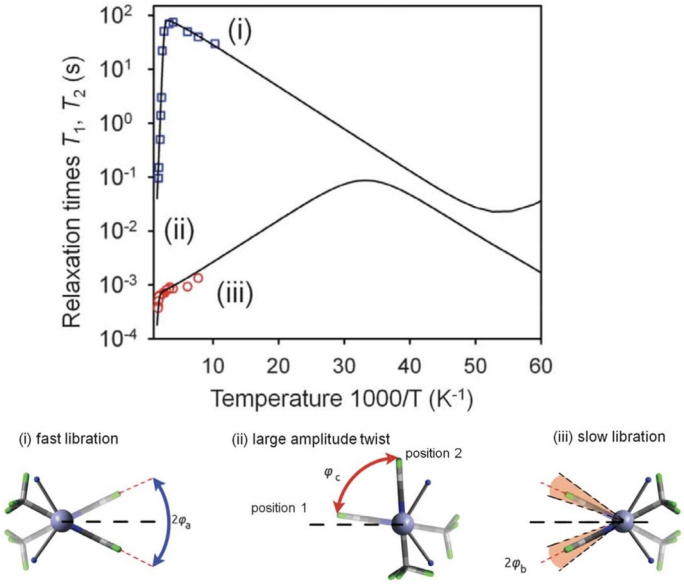

Fig. 6 Top. Variable temperature T_1 (squares) and T_2 (circles) of ^{2}H resolves framework librations in ZIF-8: (i) fast small-amplitude librations ($\varphi_a = \pm 30°$) at ~ 500 K, and much slower librations: (ii) large-amplitude twists ($\varphi_c = \pm 80° \pm 10°$) at ~ 1 Hz–$5 \times 10^4$ Hz between 300 and 600 K, and (iii) slow small-amplitude librations (φ_b). The framework defibrillates in an electric field improving the separation factor for a C_3H_6/C_3H_8 mixture by 33%. From Reference [59]

and external applied electric fields. When authors [59] tacked a ZIF-8 crystal between two electrodes and applied an electric field, gas permeation plummeted and molecular sieving capabilities peaked. They showed along with the reversible phase change between the cubic and polarized monoclinic/triclinic space groups, the linker motions stiffen, favoring propylene to permeate over propane. With variable-temperature ^{2}H NMR relaxometry, the researchers distinguished three linker motions and measured the activation energy needed to stop the high-frequency linker motion. The relaxation rates (see Fig. 6) as a function of temperature reveal the electric fields necessary to align the linker molecules.

MOF crystals are routinely imagined as being formulated within polymer matrices for use in chemical and physiological applications. A recent study showed, however, that linkers in MOF crystals rotate slower [60] when the crystals are embedded in a polymer matrix compared to those in the free crystals, or when they are amorphized [61].

With motions going on in parallel one may ask "Are they synchronous? And if yes to which extent?" The cooperative motion of neighboring phenyl likers in MIL-53 was studied wherein the authors found that replacing the functional groups on the aromatic rings directed their cooperative motion on timescales between static and 100 MHz due to linker–linker interactions [62].

While ring molecules attached to linker molecules pirouette and keep their spinning velocity invariant of the solvent [63], researchers have found that rotaxanes

shuttle on linkers between metal centers in the presence of certain guests [64]. Guest molecules that donate electrons were found to slow down linker rotations [65].

We surmise that researchers may use linker fluxionality to tune diffusion properties and promote transport of certain products or shuttle products to the next metal node for further reaction. Dynamics and control over those may be used more frequently as a design tool. NMR can help identify types of dynamics. As most sensitive to motions in the timeframe of relaxation rates R_1, R_2, and $R_{1\rho}$, the NMR spectroscopist designs their experiment based on the type of motion and velocity of interest by choice of isotope and magnetic field B_0. Thus, we expect the availability of different magnetic fields, large temperature ranges and the use of other isotopes (^{1}H, ^{2}H, ^{13}C, ^{19}F, ^{17}O) to provide animations of motions that are relevant to material properties.

5 Structure–Property Relationships

Applications of MOFs to industries such as gas storage and separations, catalytic conversion, drug delivery, and sensing, require elucidation of the distinct host–guest interactions so as to improve MOF design. The molecular level sensitivity of NMR, as highlighted in the introduction, makes NMR a unique technique to probe host–guest interactions with specificity towards adsorbent and adsorbate.

5.1 Host–Guest Interactions

Given that fossil fuel powered power plants, as well as cement and steel production, will continue to be major contributors to the world-wide CO_2 emissions, their decarbonization is of high priority to mitigate atmospheric radiative forcing. Diamine-appended MOFs offer a promising solutions to CO_2 capture from differing exhaust streams due to the tunability of adsorption isotherms based upon the chemical structure of the MOF and amine. The CO_2 adsorption mechanism, however, is not always straightforward to discern from macroscopic performance data or predict theoretically. To further elucidate the mechanism for CO_2 adsorption in one promising candidate, Mg_2(dobpdc), researchers synthesized several diamine-appended variants of a MOF and performed a comprehensive study of $^{13}CO_2$ chemisorption using ^{13}C, ^{1}H, and ^{15}N NMR spectroscopy in conjunction with Van der Walls corrected DFT calculations [66].

Van der Walls corrected DFT calculations proved particularly important to interpret the isotropic chemical shifts. The ^{1}H–^{13}C HETCOR experiment served as a fingerprint method and allowed the researchers to distinguish ammonium carbamate chains from carbamic acid pairs (see Fig. 7): The carbamic acid pairs show two strong ^{13}C–^{1}H correlations one from the adjacent NH and one from the characteristic hydrogen-bonded OH-group of the acid (see Fig. 7, bottom). In contrast, the ammonium carbamate ^{13}C HETCOR spectra also show strong ^{13}C–^{1}H correlation from the NH in the ammonium carbamate, yet only moderate dipole–dipole coupling to the ammonium protons. Interestingly, those ammonium protons charge-compensate the

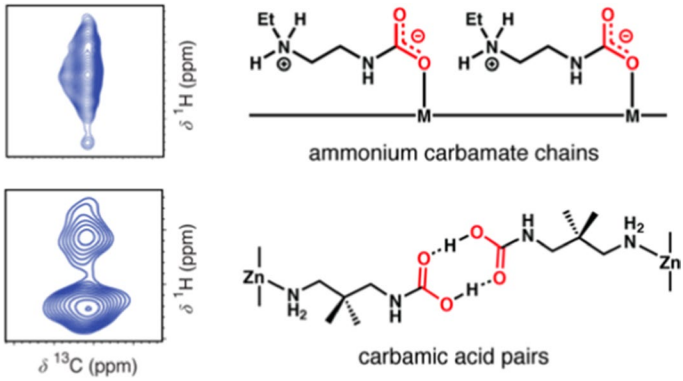

Fig. 7 2D ^{1}H–^{13}C HETCOR NMR spectra showing carbamate chain and carbamic acid pair formation [66]

emerging carbamate groups and, thus, foster a carbamate chain reaction along the pore. The onset of the carbamate chain reaction is directly correlated with reaching a threshold CO_2 partial pressure and leads to the characteristic step-shape isotherm in these materials. The researchers show 2,2-dimethyl-1,3-diaminopropane-appended Mg_2(dobdc) [67] differs from the other less bulky amines used for functionalization. This bulky diamine forms carbamic acid groups at low CO_2 concentrations that are replaced with increasing CO_2 pressure by a network of ammonium carbamate chains and carbamic acid pairs at a 1:1 ratio. The ^{13}C chemical shift ranges of carbamate and carbamic acid groups overlap and assignment of the CO_2 adsorption mechanism is not trivial, requiring carful integration of 1D and 2D NMR with calculations. Other authors demonstrate that using ^{17}O NMR from $C^{17}O_2$ -dosed MOFs effectively distinguishes carbamates from carbamic acids [68]. The chemical groups differ in their ^{17}O quadrupolar coupling constant that can be extracted from the line-shape of the ^{17}O NMR resonance of $C^{17}O_2$ allowing for unambiguous assignment of the two mechanisms.

Given that coal-fired power plants still make up a large share of CO_2 emissions world-wide, 1,2-diamino-2-methylpropane-appended Mg_2(dobpdc) offers one of the most promising solutions for an adsorbent for use in these systems. Here, workers [67] studied 1,2-diamino-2-methylpropane-appended Mg_2(dobpdc) with a step-shaped isotherm at the characteristic CO_2 partial pressure of coal-fired power plants. This diamine differs from previous amine-appended MOFs in that 1,2-diamino-2-methylpropane (dmen) leads to half of the theoretical CO_2 uptake, the reason being no preferred propagation direction of the carbamate chain. They find this half-capacity intermediate state and mixed propagation direction has a high activation barrier to transform into any of the possible full capacity states, yet full capacity is achieved by merely modifying the host MOF to an expanded pore framework form (dmen-Mg_2(p-dobpdc)). Finally, cooperative CO_2 adsorption also occurs in aminoalcohol-appended MOFs, although the mechanism is also not obvious [69]. By combining adsorption, computational, and NMR studies a cooperative distinct mechanism for a series of aminoalcohols was discovered: alcohol-appended metal

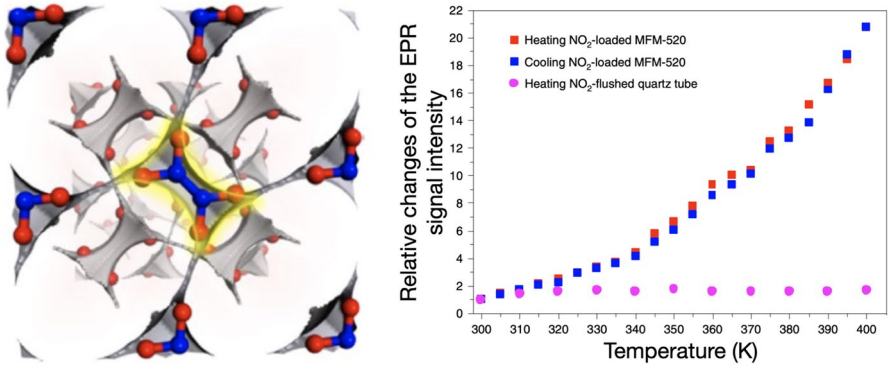

Fig. 8 In MFM-502 NO_2 dimerizes forming N_2O_4. Above room temperature N_2O_4 dissociates with a detectable EPR signal of NO_2 ($\Delta H_{dissociation} = 58$ kJ/mol). From Reference [70]

sites offer their pore-dangling amine group to form ammonium groups that charge balance the carbamate groups that form upon CO_2 adsorption.

MFM-520 effectively adsorbs NO_2 and, thus, is considered as a material for improving air quality in cities. Routine *X*-band continuous wave EPR spectroscopy at room temperature proves NO_2 is captured as a monomer in the pores [70]. At 200 K all NO_2 forms EPR-silent N_2O_4 (see Fig. 8), above 200 K N_2O_4 dissociates and NO_2 is formed, rotating and diffusing in the pores. Studying the EPR signal intensity as a function of temperature allowed the researchers to measure the enthalpy of bond dissociation of N_2O_4 (58 kJ/mol). This highlights the driving force for dimerization that results in N–N bond formation.

Ammonia is an important feedstock for industry and agriculture. But its storage and transport remain challenging due to its toxicity and corrosivity. Cu(II)-decorated defective UiO-66 serves as a top-performing NH_3 sorbent. By combining ^{1}H MAS NMR with *X*-band CW EPR, researchers [71] were able to show the direct interaction between NH_3 and Cu(II) in the MOF.

5.2 Catalysis

Due to the highly tunable porosity and large density of metal sites, MOFs have gained interest as materials for catalytic applications. The MOF Ti(IV) COK-47 presents a complex layer of TiO_6 and 2D structural building units [72]. Determination of ^{13}C chemical shifts with DFT calculations demonstrated (see Fig. 9) the presence of a temperature-induced transition from bridging methoxides to terminal methoxides, with these terminal groups showing excellent catalytic activity for oxidation of dibenzothiophene. EPR on these materials was also performed to confirm the presence of a Ti(III).

MOF-based single-atom catalysts have shown great potential in a variety of reactions, but the identification of the atomically dispersed metal sites and the elucidation of the mechanism remain challenging. Combined in situ and operando NMR and EPR showed [73] the location of atomically dispersed Cu sites in UiO-66. When

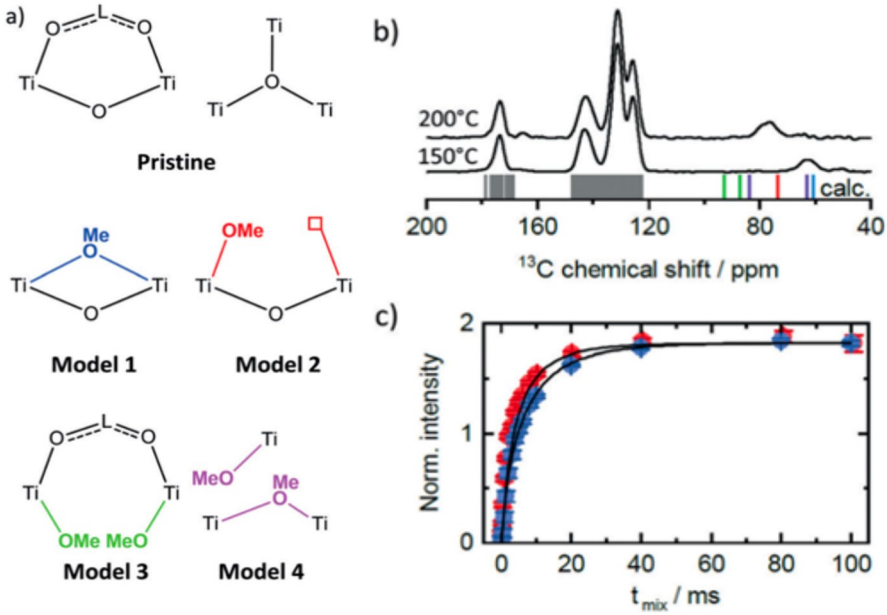

Fig. 9 Different possible purposed Ti–O–Me structures for COK-47, the ^{13}C chemical shift for each structure was determined using DFT. This calculated ^{13}C chemical shift for each Me–O structure is shown in (**b**) and compared with the experimentally measured spectrum in black at two different temperatures 150 and 200 °C. A transition can be seen with increasing temperature from model 1 to model 2. [72]

analyzed alongside diffraction methods, these authors showed that single-atom Cu is coordinated to –OH/–OH_2 defect sites. The role of Cu sites in the adsorption and activation of NO_2 was further revealed by solid-state NMR that demonstrated that the adsorption of NO_2 occurs at the Cu and hydroxyl sites.

Acidic sites in solid acid catalysts have been an active area of investigation for decades owing to their importance in a variety of industries. The origin of acidity in MOF-808-SO_4 was revealed [74] experimentally by a series of solid-state NMR studies, notably with high speed proton MAS. The structure of the acid was elucidated and found to be the pairing of two bases (chelating sulfate and μ^1-OH) supported on two neighboring zirconium atoms and sharing a weakly bound proton between them.

6 Materials by Design

A Holy Grail in materials research is the computational design of materials for a specific purpose, then realization of that design both synthetically and functionally. NMR provided the first proof of concept for a computationally designed material for CO_2 separation from power plant flue gas [75]. Many MOFs perform well in

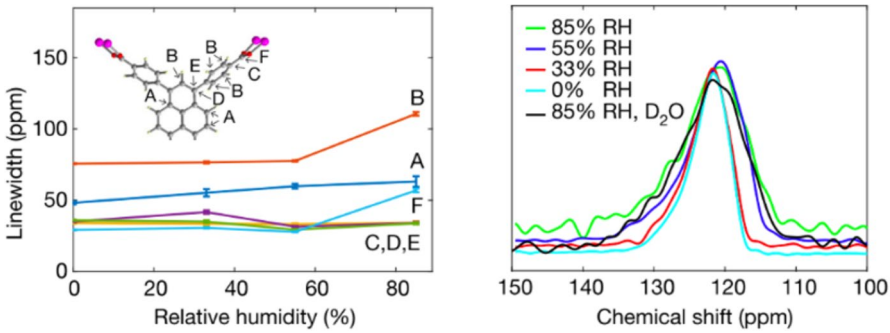

Fig. 10 ^{13}C CP MAS NMR spectroscopy of Al-PyrMOF, a MOF created to adsorb CO_2 at the exclusion of water. Left: c linewidths assigned to carbon sites **A**–**F**; Right: static spectrum of adsorbed CO_2 as a function of relative humidity

separating CO_2 from N_2 but fail in the presence of water vapor where water outperforms CO_2 in competition for the same adsorption sites.

Where pharmacologists scan protein active binding pockets—the pharmacophores—for drug molecules, these authors reversed the concept. The small "drug molecule" CO_2 was known, and they computationally screened 325,000 potential MOF structures as candidates for CO_2 adsorption ("binding pockets") and added an additional constraint of low water uptake. Of the screened MOFs, 8325 had high CO_2/N_2 selectivity and high capacities for CO_2. The researchers found three structural types for that active binding pockets and named adsorbaphores for CO_2 capture. One of these adsorbaphores computationally presented low water uptake: structures with 0.65–0.7 nm-spaced parallel aromatic rings. Upon dosing Al-PyrMOF with CO_2 at relative humidity of 0–85%, the ^{13}C CP MAS NMR spectra of linker carbons reflect minimal broadening in the presence of co-adsorbed water; the adsorption site adjacent to the carboxylate group (Site B, see Fig. 10) changed modestly in linewidth only at the very highest relative humidity of 85% tested. Static spectra from adsorbed $^{13}CO_2$ showed minimal linewidth changes in the presence of varying amounts of H_2O (and D_2O), affirming the design principle that the adsorbaphore excludes water. Their study verifies the utility of the de novo creation of a material for a given separation problem.

7 Conclusions

Magnetic resonance spectroscopy adds value to MOF research in various ways, including monitoring crystal growth to ascertain mechanisms for synthesis, measuring adsorption isotherms with spectroscopically resolved site resolution, and aiding in the discovery of a new material class, MOF glasses. In the last 5.5 years, researchers discovered with the help of MR spectroscopy new phenomena in MOFs and gained experimental evidence for chemical mechanism, including: linker dynamics in ZIF-8 that defibrillate in an electric field [59] (NMR); CO_2 adsorption

in diamine-appended Mg_2(dobdc) via carbamate-chains (theoretically proposed in 2015), carbamic acid pairs, or a mixed adsorption mechanism [66]; NO_2 dimerization in MFM-502 designed for clean air [70] (EPR); and the speciation of atomic sites for catalysis [72, 73].

The studies share one underlying pattern: the creative use of two features of MR: the long lifetimes that afford interrogation of nuclear spins to yield desired parameters, and the control of the phase of *rf* pulses so as design coherence transfer pathways to minimize artifacts and afford observation of quadrupolar nuclei such as ^{17}O. Our review shows that between 01/2017 and 07/2022, there have been ~ 450 studies of MOFs with NMR. We expect high quality, and creative research on MOFs using MR in future years given the profile these materials exhibit in fundamental and applied research and technology. We propose that MR methods must adapt to rising new questions in MOF research and focus where the effort is warranted. Possible examples may be upscaled MOF synthesis with the reactor in the magnetic field or MR sensing volume, new materials in the form of composites and structured systems (e.g., mixed matrix membranes of core–shell structures), MOFs with paramagnetic ions, and MOFs tailored to special applications such as food science, health care, and sensing.

Future researchers will likely further exploit relaxometry so as to unravel details and energetics of motion, both in MOFs and of materials imbibed within them. Emerging solids NMR methods that can further MR studies of MOFs include fast spinning Magic Angle Spinning (MAS) to research MOFs with paramagnetic ions [76], Dynamic Nuclear Polarization (DNP) to assess radicals on linkers and study of crystal growth, as use of high magnetic fields (e.g., ^{17}O NMR at very high fields) [77, 78] or DNP [79] to study the structure and properties of MOFs.

7.1 Methods

We searched the databases Scopus and Web of Science Core Collection on 08/22/2022, searching for "metal organic framework" AND "NMR;" we added "solid-state NMR" as an additional search filter. For the first search, we eliminated by hand false positives finding where liquids NMR was only used for standard linker characterization. Table 2 summarizes the employed filter criteria. One major decision for the focus of this research is the definition of key challenges in the field of metal–organic research for material improvements that we define in the introduction and use as a filter. We found 450 for MOF + solid-state NMR published in between 01/2017 and 07/2022 all written in English language (1312 articles for MOF + NMR without the solid-state filter). Widening our search to NMR and EPR and applying the same filter we find 124 articles between 2017 and 2022 in magnetic resonance: distributed to the sub challenges as follow (number in parenthesis show share of EPR studies): 31 (8) in Structure, 18 (1) in Synthesis, 27 (4) in Dynamics, 46 (13) in Properties, and 2 (0) in Functionality. This signifies all fields are active and emerging fields of research.

Table 2 Criteria

	Included	Excluded
Search criteria	"Metal organic framework" AND "solid-state NMR"	Only liquids NMR
Dates	01/2017–07/2022	Before 2017 and after 08/01/2022
Literature sources	Articles in peer-reviewed journals	Gray literature
Selection Criterion (SC) 1	NMR has significant contribution	NMR with minor contribution
SC 1a—Contribution to field	Contribution to key challenges in MOF research (defined in Fig. 1)	Only minor contribution to those challenges
SC 1b—Necessity of NMR features	Essential role of NMR cannot be replaced by methods that are usually cheaper	NMR contribution could have easily been replaced by other method
SC2—Tailoring	NMR approach customized to problem	NMR not tailored to research question
SC3—Execution	Great execution of NMR approach	Poor execution of NMR approach

Acknowledgements The work was prepared for the Applied Magnetic Resonance issue on the occasion of Bernhard Blümich's 70th birthday. The authors acknowledge support for their research from the PrISMa Project (No. 299659) that funded through the ACT program (Accelerating CCS Technologies, Horizon2020 Project No. 294766). The PrISMa project consisted of financial contributions made from the Department for Business, Energy & Industrial Strategy (BEIS) together with extra funding from the NERC and EPSRC research councils, United Kingdom; The Research Council of Norway, (RCN), Norway; the Swiss Federal Office of Energy (SFOE), Switzerland; and the US-Department of Energy (US-DOE), USA. LMF, HZ and JAR further acknowledge support from the U.S. Department of Energy Office of Basic Energy Sciences under award DE-SC0019992.

Author Contributions All authors created and edited content.

Data Availability Not applicable.

Declarations

Conflict of Interest None.

Ethical Approval Not applicable.

Open Access This article is licensed under a Creative Commons Attribution 4.0 International License, which permits use, sharing, adaptation, distribution and reproduction in any medium or format, as long as you give appropriate credit to the original author(s) and the source, provide a link to the Creative Commons licence, and indicate if changes were made. The images or other third party material in this article are included in the article's Creative Commons licence, unless indicated otherwise in a credit line to the material. If material is not included in the article's Creative Commons licence and your intended use is not permitted by statutory regulation or exceeds the permitted use, you will need to obtain permission directly from the copyright holder. To view a copy of this licence, visit http://creativecommons.org/licenses/by/4.0/.

References

1. H. Furukawa, K.E. Cordova, M. O'Keeffe, O.M. Yaghi, The chemistry and applications of metal-organic frameworks. Science (80-) **341**(6149), 1230444 (2013). https://doi.org/10.1126/science.1230444
2. H. Furukawa, N. Ko, Y.B. Go, N. Aratani, S.B. Choi, E. Choi, A.Ö. Yazaydin, R.Q. Snurr, M. O'Keeffe, J. Kim, O.M. Yaghi, Ultrahigh porosity in metal-organic frameworks. Science (80-) **329**(5990), 424–428 (2010). https://doi.org/10.1126/science.1192160
3. T. Wang, E. Lin, Y.L. Peng, Y. Chen, P. Cheng, Z.J. Zhang, Rational design and synthesis of ultramicroporous metal-organic frameworks for gas separation. Coord. Chem. Rev. **423**, 213485 (2020)
4. Q. Qian, P.A. Asinger, M.J. Lee, G. Han, K.M. Rodriguez, S. Lin, F.M. Benedetti, A.X. Wu, W.S. Chi, Z.P. Smith, MOF-based membranes for gas separations. Chem. Rev. **120**, 8161–8266 (2020)
5. F. Lorignon, A. Gossard, M. Carboni, Hierarchically porous monolithic MOFs: an ongoing challenge for industrial-scale effluent treatment. Chem. Eng. J. **393**, 124764 (2020)
6. Qi. Wang, Q. Gao, A.M. Al-Enizi, A. Nafady, S. Ma, Recent advances in MOF-based photocatalysis: environmental remediation under visible light. Inorg. Chem. Front. **7**, 300 (2020)
7. H. Furukawa, U. Müller, O.M. Yaghi, "Heterogeneity within order" in metal-organic frameworks. Angew. Chemie Int. Ed. **54**(11), 3417–3430 (2015). https://doi.org/10.1002/anie.201410252
8. Y. Wu, D. Wang, Y. Li, Understanding of the major reactions in solution synthesis of functional nanomaterials. Sci. China Mater. **59**(11), 938–996 (2016). https://doi.org/10.1007/s40843-016-5112-0
9. J. Kärger, Transport phenomena in nanoporous materials. ChemPhysChem **16**(1), 24–51 (2015). https://doi.org/10.1002/cphc.201402340

10. J. Park, J.D. Howe, D.S. Sholl, How reproducible are isotherm measurements in metal-organic frameworks? Chem. Mater. **29**(24), 10487–10495 (2017). https://doi.org/10.1021/acs.chemmater.7b04287
11. P.G. Boyd, Y. Lee, B. Smit, Computational development of the nanoporous materials genome. Nat. Rev. Mater. **2**(8), 1–15 (2017). https://doi.org/10.1038/natrevmats.2017.37
12. S. Furukawa, J. Reboul, S. Diring, K. Sumida, S. Kitagawa, Structuring of metal-organic frameworks at the mesoscopic/macroscopic scale. Chem. Soc. Rev. **43**(16), 5700–5734 (2014). https://doi.org/10.1039/c4cs00106k
13. J. Ren, M. Ledwaba, N.M. Musyoka, H.W. Langmi, M. Mathe, S. Liao, W. Pang, Structural defects in metal-organic frameworks (MOFs): formation, detection and control towards practices of interests. Coord. Chem. Rev. **349**, 169–197 (2017). https://doi.org/10.1016/j.ccr.2017.08.017
14. A. Abragam, *The principles of nuclear magnetism* (Oxford Univerty Press, Oxford, 1961)
15. G.P.M. Bignami, Z.H. Davis, D.M. Dawson, S.A. Morris, S.E. Russell, D. McKay, R.E. Parke, D. Iuga, R.E. Morris, S.E. Ashbrook, Cost-Effective 17O enrichment and NMR spectroscopy of mixed-metal terephthalate metal-organic frameworks. Chem. Sci. **9**(4), 850–859 (2018). https://doi.org/10.1039/c7sc04649a
16. G. Mali, M. Mazaj, I. Arčon, D. Hanžel, D. Arčon, Z. Jagličić, Unraveling the arrangement of Al and Fe within the framework explains the magnetism of mixed-metal MIL-100(Al, Fe). J. Phys. Chem. Lett. **10**(7), 1464–1470 (2019). https://doi.org/10.1021/acs.jpclett.9b00341
17. K.C. Jayachandrababu, D.S. Sholl, S. Nair, Structural and mechanistic differences in mixed-linker zeolitic imidazolate framework synthesis by solvent assisted linker exchange and de novo routes. J. Am. Chem. Soc. **139**(16), 5906–5915 (2017). https://doi.org/10.1021/jacs.7b01660
18. B. Bueken, D. De Vos, A.A. Krajnc, B. Bueken, D. De Vos, G. Mali, Improved resolution and simplification of the spin-diffusion-based NMR method for the structural analysis of mixed-linker MOFs. J. Magn. Reson. **279**, 22–28 (2017). https://doi.org/10.1016/j.jmr.2017.04.008
19. B. Bueken, N. Van Velthoven, A. Krajnc, S. Smolders, F. Taulelle, C. Mellot-Draznieks, G. Mali, T.D. Bennett, D. De Vos, Tackling the defect conundrum in UiO-66: a mixed-linker approach to engineering missing linker defects. Chem. Mater. **29**(24), 10478–10486 (2017). https://doi.org/10.1021/acs.chemmater.7b04128
20. N. Tien-Binh, D. Rodrigue, S. Kaliaguine, In-situ cross interface linking of PIM-1 polymer and UiO-66-NH2 for outstanding gas separation and physical aging control. J. Memb. Sci. **548**, 429–438 (2018). https://doi.org/10.1016/j.memsci.2017.11.054
21. Y. Peng, V. Krungleviciute, I. Eryazici, J.T. Hupp, O.K. Farha, T. Yildirim, Methane storage in metal-organic frameworks: current records, surprise findings, and challenges. J. Am. Chem. Soc. **135**(32), 11887–11894 (2013). https://doi.org/10.1021/JA4045289
22. S.E. Morgan, A.M. O'Connell, A. Jansson, G.W. Peterson, J.J. Mahle, T.B. Eldred, W. Gao, G.N. Parsons, Stretchable and multi-metal–organic framework fabrics via high-yield rapid sorption-vapor synthesis and their application in chemical warfare agent hydrolysis. ACS Appl. Mater. Interfaces **13**(26), 31279–31284 (2021). https://doi.org/10.1021/ACSAMI.1C07366
23. J. Li, X. Wang, G. Zhao, C. Chen, Z. Chai, A. Alsaedi, T. Hayat, X. Wang, Metal-organic framework-based materials: superior adsorbents for the capture of toxic and radioactive metal ions. Chem. Soc. Rev. **47**(7), 2322–2356 (2018). https://doi.org/10.1039/C7CS00543A
24. M. Ding, R.W. Flaig, H.-L. Jiang, O.M. Yaghi, Carbon capture and conversion using metal-organic frameworks and MOF-based materials. Chem. Soc. Rev. **48**(10), 2783–2828 (2019). https://doi.org/10.1039/C8CS00829A
25. K. Ma, T. Islamoglu, Z. Chen, P. Li, M.C. Wasson, Y. Chen, Y. Wang, G.W. Peterson, J.H. Xin, O.K. Farha, Scalable and template-free aqueous synthesis of zirconium-based metal-organic framework coating on textile fiber. J. Am. Chem. Soc. **141**(39), 15626–15633 (2019). https://doi.org/10.1021/JACS.9B07301
26. J. Hou, C.W. Ashling, S.M. Collins, A. Krajnc, C. Zhou, L. Longley, D.N. Johnstone, P.A. Chater, S. Li, M.-V. Coulet, P.L. Llewellyn, F.-X. Coudert, D.A. Keen, P.A. Midgley, G. Mali, V. Chen, T.D. Bennett, Metal-organic framework crystal-glass composites. Nat. Commun. (2019). https://doi.org/10.1038/s41467-019-10470-z
27. D. Umeyama, N.P. Funnell, M.J. Cliffe, J.A. Hill, A.L. Goodwin, Y. Hijikata, T. Itakura, T. Okubo, S. Horike, S. Kitagawa, Glass formation via structural fragmentation of a 2D coordination network. Chem. Commun. **51**(64), 12728–12731 (2015). https://doi.org/10.1039/c5cc04626b
28. T.D. Bennett, Y. Yue, P. Li, A. Qiao, H. Tao, N.G. Greaves, T. Richards, G.I. Lampronti, S.A.T. Redfern, F. Blanc, O.K. Farha, J.T. Hupp, A.K. Cheetham, D.A. Keen, Melt-quenched glasses of

metal-organic frameworks. J. Am. Chem. Soc. **138**(10), 3484–3492 (2016). https://doi.org/10.1021/jacs.5b13220
29. D. Umeyama, S. Horike, M. Inukai, T. Itakura, S. Kitagawa, Reversible solid-to-liquid phase transition of coordination polymer crystals. J. Am. Chem. Soc. **137**(2), 864–870 (2015). https://doi.org/10.1021/ja511019u
30. T.D. Bennett, J.C. Tan, Y. Yue, E. Baxter, C. Ducati, N.J. Terrill, H.H.M. Yeung, Z. Zhou, W. Chen, S. Henke, A.K. Cheetham, G.N. Greaves, Hybrid glasses from strong and fragile metal-organic framework liquids. Nat. Commun. **6**, 1–7 (2015). https://doi.org/10.1038/ncomms9079
31. Y. Zhao, S.Y. Lee, N. Becknell, O.M. Yaghi, C.A. Angell, Nanoporous transparent MOF glasses with accessible internal surface. J. Am. Chem. Soc. **138**(34), 10818–10821 (2016). https://doi.org/10.1021/jacs.6b07078
32. C. Zhou, L. Longley, A.A. Krajnc, G.J. Smales, A. Qiao, I. Erucar, C.M. Doherty, A.W. Thornton, A.J. Hill, C.W. Ashling, O.T. Qazvini, S.J. Lee, P.A. Chater, N.J. Terrill, A.J. Smith, Y. Yue, G. Mali, D.A. Keen, S.G. Telfer, T.D. Bennett, Metal-organic framework glasses with permanent accessible porosity. Nat. Commun. **9**(1), 1–9 (2018). https://doi.org/10.1038/s41467-018-07532-z
33. R.S.K. Madsen, A. Qiao, J. Sen, I. Hung, K. Chen, Z. Gan, S. Sen, Y. Yue, Ultrahigh-field 67 Zn NMR reveals short-range disorder in zeolitic imidazolate framework glasses. Science **1476**(March), 1473–1476 (2020)
34. T.M.M. Ntep, H. Breitzke, L. Schmolke, C. Schlüsener, B. Moll, S. Millan, N. Tannert, I. El Aita, G. Buntkowsky, C. Janiak, T.M.M. Ntep, H. Breitzke, L. Schmolke, C. Schluesener, B. Moll, S. Millan, N. Tannert, I. El Aita, G. Buntkowsky, C. Janiak, Facile in situ halogen functionalization via triple-bond hydrohalogenation: enhancing sorption capacities through halogenation to halofumarate-based Zr(IV)-metal-organic frameworks. Chem. Mater. **31**(21), 8629–8638 (2019). https://doi.org/10.1021/acs.chemmater.9b00524
35. J. Hou, M.L. Ríos Gómez, A. Krajnc, A. McCaul, S. Li, A.M. Bumstead, A.F. Sapnik, Z. Deng, R. Lin, P.A. Chater, D.S. Keeble, D.A. Keen, D. Appadoo, B. Chan, V. Chen, G. Mali, T.D. Bennett, halogenated metal-organic framework glasses and liquids. J. Am. Chem. Soc. **142**(8), 3880–3890 (2020). https://doi.org/10.1021/jacs.9b11639
36. P. Duan, J.C. Moreton, S.R. Tavares, R. Semino, G. Maurin, S.M. Cohen, K. Schmidt-Rohr, Polymer infiltration into metal-organic frameworks in mixed-matrix membranes detected in situ by NMR. J. Am. Chem. Soc. **141**(18), 7589–7595 (2019). https://doi.org/10.1021/jacs.9b02789
37. C.L. Jones, C.E. Hughes, H.H.M. Yeung, A. Paul, K.D.M. Harris, T.L. Easun, Exploitingin situNMR to monitor the formation of a metal-organic framework. Chem. Sci. **12**(4), 1486–1494 (2021). https://doi.org/10.1039/d0sc04892e
38. C.A. O'Keefe, C. Mottillo, J. Vainauskas, L. Fabian, T. Friscic, R.W. Schurko, NMR-enhanced crystallography aids open metal-organic framework discovery using solvent-free accelerated aging. Chem. Mater. **32**(10), 4273–4281 (2020). https://doi.org/10.1021/acs.chemmater.0c00894
39. D.A. Levenson, J.F. Zhang, P.M.J. Szell, D.L. Bryce, B.S. Gelfand, R.P.S. Huynh, N.D. Fylstra, G.K.H. Shimizu, Effects of secondary anions on proton conduction in a flexible cationic phosphonate metal-organic framework. Chem. Mater. **32**(2), 679–687 (2020). https://doi.org/10.1021/acs.chemmater.9b03453
40. S. Krause, V. Bon, I. Senkovska, U. Stoeck, D. Wallacher, D.M. Többens, S. Zander, R.S. Pillai, G. Maurin, F.-X. Coudert, S. Kaskel, A pressure-amplifying framework material with negative gas adsorption transitions. Nature **532**, 348–352 (2016). https://doi.org/10.1038/nature17430
41. S. Krause, F.S. Reuter, S. Ehrling, V. Bon, I. Senkovska, S. Kaskel, E. Brunner, Impact of defects and crystal size on negative gas adsorption in DUT-49 analyzed by in situ 129Xe NMR spectroscopy. Chem. Mater. **32**(11), 4641–4650 (2020). https://doi.org/10.1021/acs.chemmater.0c01059
42. S. Chen, Z. Song, J. Lyu, Y. Guo, B.E.G. Lucier, W. Luo, M.S. Workentin, X. Sun, Y. Huang, Anhydride post-synthetic modification in a hierarchical metal-organic framework. J. Am. Chem. Soc. **142**(9), 4419–4428 (2020). https://doi.org/10.1021/jacs.9b13414
43. J.J.O. Marreiros, R. De Oliveira-Silva, P. Iacomi, P.L. Llewellyn, R. Ameloot, D. Sakellariou, Benchtop in situ measurement of full adsorption isotherms by NMR. J. Am. Chem. Soc **143**(22), 8249–8254 (2021). https://doi.org/10.1021/jacs.1c03716
44. M. Sin, C. Kutzscher, I. Senkovska, T. Ben, S. Qiu, S. Kaskel, E. Brunner, Surface polarity estimation of metal-organic frameworks using liquid-phase mixture adsorption. Microporous Mesoporous Mater. **251**, 129–134 (2017)
45. S. Krause, B.L. Feringa, Towards artificial molecular factories from framework-embedded molecular machines. Nat. Rev. Chem. **4**(10), 550–562 (2020). https://doi.org/10.1038/s41570-020-0209-9

46. N. Dvoyashkina, D. Freude, S.S. Arzumanov, A.G. Stepanov, Monitoring the diffusivity of light hydrocarbons in a mixture by magic angle spinning pulsed field gradient NMR: methane/ethane/ethene in ZIF-8. J. Phys. Chem. C **121**(45), 25372–25376 (2017). https://doi.org/10.1021/acs.jpcc.7b09335
47. A. Dutta, N. Tymińska, G. Zhu, J. Collins, R.P. Lively, J.R. Schmidt, S. Vasenkov, N. Tyminska, G. Zhu, J. Collins, R.P. Lively, J.R. Schmidt, S. Vasenkov, Influence of hydrogen sulfide exposure on the transport and structural properties of the metal-organic framework ZIF-8. J. Phys. Chem. C **122**(13), 7278–7287 (2018). https://doi.org/10.1021/acs.jpcc.8b00798
48. M.I. Velasco, R.H. Acosta, W.A. Marmisollé, O. Azzaroni, M. Rafti, Modulation of hydrophilic/hydrophobic character of porous environments in metal-organic frameworks via direct polymer capping probed by NMR diffusion measurements. J. Phys. Chem. C **123**(34), 21076–21082 (2019). https://doi.org/10.1021/acs.jpcc.9b06824
49. V.J. Witherspoon, R. Mercado, E. Braun, A. Mace, J. Bachman, J.R. Long, B. Blümich, B. Smit, J.A. Reimer, Combined nuclear magnetic resonance and molecular dynamics study of methane adsorption in M_2(dobdc) metal-organic frameworks. J. Phys. Chem. C **123**(19), 12286–12295 (2019). https://doi.org/10.1021/ACS.JPCC.9B01733
50. A.C. Forse, M.I. Gonzalez, R.L. Siegelman, V.J. Witherspoon, S. Jawahery, R. Mercado, P.J. Milner, J.D. Martell, B. Smit, B. Blümich, J.R. Long, J.A. Reimer, B. Bluemich, J.R. Long, J.A. Reimer, B. Blümich, J.R. Long, J.A. Reimer, Unexpected diffusion anisotropy of carbon dioxide in the metal-organic framework Zn_2(dobpdc). J. Am. Chem. Soc. **140**(5), 1663–1673 (2018). https://doi.org/10.1021/jacs.7b09453
51. A.C. Forse, K.A. Colwell, M.I. Gonzalez, S. Benders, R.M. Torres-Gavosto, B. Blümich, J.A. Reimer, J.R. Long, Influence of pore size on carbon dioxide diffusion in two isoreticular metal-organic frameworks. Chem. Mater. **32**, 3570–3576 (2020). https://doi.org/10.1021/acs.chemmater.0c00745
52. R.M. Marti, J.D. Howe, C.R. Morelock, M.S. Conradi, K.S. Walton, D.S. Sholl, S.E. Hayes, CO2 dynamics in pure and mixed-metal MOFs with open metal sites. J. Phys. Chem. C **121**(39), 25778–25787 (2017). https://doi.org/10.1021/acs.jpcc.7b07179
53. Y. Lu, B.E.G. Lucier, Y. Zhang, P. Ren, A. Zheng, Y. Huang, Sizable dynamics in small pores: CO_2 location and motion in the α-Mg formate metal-organic framework. Phys. Chem. Chem. Phys. **19**(8), 6130–6141 (2017). https://doi.org/10.1039/c7cp00199a
54. M. Inukai, T. Kurihara, Y. Noda, W.M. Jiang, K. Takegoshi, N. Ogiwara, H. Kitagawa, K. Nakamura, Probing dynamics of carbon dioxide in a metal-organic framework under high pressure by high-resolution solid-state NMR. Phys. Chem. Chem. Phys. **22**(26), 14465–14470 (2020). https://doi.org/10.1039/d0cp01216e
55. J. Xu, Y.M. Liu, A.S. Lipton, J. Ye, G.L. Hoatson, P.J. Milner, T.M. McDonald, R.L. Siegelman, A.C. Forse, B. Smit, J.R. Long, J.A. Reimer, Amine dynamics in diamine-appended Mg2(Dobpdc) metal-organic frameworks. J. Phys. Chem. Lett. **10**(22), 7044–7049 (2019). https://doi.org/10.1021/acs.jpclett.9b02883
56. R. Giovine, C. Volkringer, M.-A.A.M.-A. Springuel-Huet, A. Nossov, F.F.F. Blanc, J. Trébosc, T. Loiseau, J.P.J.-P. Amoureux, O. Lafon, F.F. Pourpoint, J. Trebosc, T. Loiseau, J.-P. Arnoureux, O. Lafon, F.F. Pourpoint, Study of xenon mobility in the two forms of MIL-53(Al) using solid-state NMR spectroscopy. J. Phys. Chem. C **121**(35), 19262–19268 (2017). https://doi.org/10.1021/acs.jpcc.7b06006
57. R. Zettl, S. Lunghammer, B. Gadermaier, A. Boulaoued, P. Johansson, H.M.R. Wilkening, I. Hanzu, High Li+ and Na+ conductivity in new hybrid solid electrolytes based on the porous MIL-121 metal organic framework. Adv. Energy Mater. (2021). https://doi.org/10.1002/aenm.202003542
58. M.K. Sarango-Ramirez, D.W. Lim, D.I. Kolokolov, A.E. Khudozhitkov, A.G. Stepanov, H. Kitagawa, Superprotonic conductivity in metal-organic framework via solvent-free coordinative urea insertion. J. Am. Chem. Soc. **142**(15), 6861–6865 (2020). https://doi.org/10.1021/jacs.0c00303
59. A. Knebel, B. Geppert, K. Volgmann, D.I. Kolokolov, A.G. Stepanov, J. Twiefel, P. Heitjans, D. Volkmer, J. Caro, Defibrillation of soft porous metal-organic frameworks with electric fields. Science (80-) **358**(6361), 347–351 (2017)
60. S. Friebe, A. Mundstock, K. Volgmann, J.J. Caro, On the better understanding of the surprisingly high performance of metal-organic framework-based mixed-matrix membranes using the example of UiO-66 and matrimid. ACS Appl. Mater. Interfaces **9**(47), 41553–41558 (2017). https://doi.org/10.1021/acsami.7b13037

61. N. Ogiwara, D.I. Kolokolov, M. Donoshita, H. Kobayashi, S. Horike, A.G. Stepanov, H. Kitagawa, The effect of amorphization on the molecular motion of the 2-methylimidazolate linkers in ZIF-8. Chem. Commun. **55**(42), 5906–5909 (2019). https://doi.org/10.1039/C9CC02673H
62. A. Gonzalez-Nelson, S. Mula, M. Šimėnas, S. Balčiūnas, A.R. Altenhof, C.S. Vojvodin, J. Banys, R.W. Schurko, F.-X. Coudert, M.A. Van Der Veen, Emergence of coupled rotor dynamics in metal-organic frameworks via tuned steric interactions; 21. J. Am. Chem. Soc. **143**(31), 12053–12062 (2021). https://doi.org/10.1021/jacs.1c03630
63. P. Martinez-Bulit, C.A. O'Keefe, K. Zhu, R.W. Schurko, S.J. Loeb, C.A.O. Keefe, K. Zhu, R.W. Schurko, S.J. Loeb, Solvent and steric influences on rotational dynamics in porphyrinic metal-organic frameworks with mechanically interlocked pillars. Cryst. Growth Des. **19**(10), 5679–5685 (2019). https://doi.org/10.1021/acs.cgd.9b00669
64. B.H. Wilson, L.M. Abdulla, R.W. Schurko, S.J. Loeb, Translational dynamics of a non-degenerate molecular shuttle imbedded in a zirconium metal-organic framework. Chem. Sci. **12**(11), 3944–3951 (2021). https://doi.org/10.1039/d0sc06837c
65. A.E. Khudozhitkov, H. Jobic, D.I. Kolokolov, D. Freude, J. Haase, A.G. Stepanov, Probing the guest-mediated structural mobility in the UiO-66(Zr) framework by 2H NMR spectroscopy. J. Phys. Chem. C **121**(21), 11593–11600 (2017). https://doi.org/10.1021/acs.jpcc.7b03259
66. A.C. Forse, P.J. Milner, J.H. Lee, H.N. Redfearn, J. Oktawiec, R.L. Siegelman, J.D. Martell, B. Dinakar, L.B. Porter-Zasada, M.I. Gonzalez, J.B. Neaton, J.R. Long, J.A. Reimer, Elucidating CO_2 chemisorption in diamine-appended metal-organic frameworks. J. Am. Chem. Soc. **140**(51), 18016–18031 (2018). https://doi.org/10.1021/jacs.8b10203
67. B. Dinakar, A.C. Forse, H.Z.H. Jiang, Z.T. Zhu, J.H. Lee, E.J. Kim, S.T. Parker, C.J. Pollak, R.L. Siegelman, P.J. Milner, J.A. Reimer, J.R. Long, Overcoming metastable CO_2 adsorption in a bulky diamine-appended metal-organic framework. J. Am. Chem. Soc. **143**(37), 15258–15270 (2021). https://doi.org/10.1021/jacs.1c06434
68. A.H. Berge, S.M. Pugh, M.I.M. Short, Z. Lu, J.-H. Lee, C.J. Pickard, A.C. Forse, Revealing carbon capture chemistry with 17-oxygen NMR spectroscopy. Nat. Commun. **13**, 7763 (2022). https://doi.org/10.1038/s41467-022-35254-w
69. V.Y. Mao, P.J. Milner, J.-H. Lee, A.C. Forse, E.J. Kim, R.L. Siegelman, C. Michael McGuirk, L.B. Porter-Zasada, J.B. Neaton, J.A. Reimer, J.R. Long, Cooperative carbon dioxide adsorption in alcoholamine- and alkoxyalkylamine-functionalized metal-organic frameworks. Angew. Chem. Int. Ed. Engl. **59**(44), 19468–19477 (2020). https://doi.org/10.1002/ANIE.201915561
70. J. Li, X. Han, X. Zhang, A.M. Sheveleva, Y. Cheng, F. Tuna, E.J.L.L. McInnes, L.J.M. Mcpherson, S.J. Teat, L.L. Daemen, A.J. Ramirez-cuesta, M. Schröder, S. Yang, L.J. McCormick McPherson, S.J. Teat, L.L. Daemen, A.J. Ramirez-cuesta, M. Schröder, S. Yang, Capture of nitrogen dioxide and conversion to nitric acid in a porous metal-organic framework. Nat. Chem. **11**(12), 1085–1090 (2019). https://doi.org/10.1038/s41557-019-0356-0
71. Y. Ma, X. Han, X. Shaojun, Z. Wang, W. Li, I. da Silva, S. Chansai, D. Lee, Y. Zou, M. Nikiel, P. Manuel, A.M. Sheveleva, F. Tuna, E.J.L. McInnes, Y. Cheng, S. Rudic, A.J. Ramirez-Cuesta, S.J. Haigh, C. Hardacre, M. Schröder, S. Yang, Atomically dispersed copper sites in a metal−organic framework for reduction of nitrogen dioxide. J. Am. Chem. Soc. **143**, 10977–10985 (2021). https://doi.org/10.1021/jacs.1c03036
72. S. Smolders, T. Willhammar, A.A. Krajnc, K. Sentosun, M.T. Wharmby, K.A. Lomachenko, S. Bals, G. Mali, M.B.J.J. Roeffaers, D.E. De Vos, B. Bueken, A titanium(IV)-based metal-organic framework featuring defect-rich Ti-O sheets as an oxidative desulfurization catalyst. Angew. Cheme IE **58**(27), 9160–9165 (2019). https://doi.org/10.1002/anie.201904347
73. Y. Ma, X. Han, S. Xu, Z. Wang, W. Li, I. da Silva, S. Chansai, D. Lee, Y. Zou, M. Nikiel, P. Manuel, A.M. Sheveleva, F. Tuna, E.J.L. McInnes, Y. Cheng, S. Rudic, A.J. Ramirez-Cuesta, S.J. Haigh, C. Hardacre, C. Schröder, S. Yang, Atomically dispersed copper sites in a metal−organic framework for reduction of nitrogen dioxide. J. Am. Chem. Soc. **143**, 10977–10985 (2021). https://doi.org/10.1021/jacs.1c03036
74. C.A. Trickett, T.M. Osborn, J.S. Popp, C. Yan, J. Weisberg, A. Huq, P. Urban, J. Jiang, M.J. Kalmutzki, Q. Liu, J. Baek, M.P. Head-Gordon, G.A. Somorjai, J.A. Reimer, O.M. Yaghi, Identification of the strong Brønsted acid site in a metal–organic framework solid acid catalyst. Nat. Chem. **11**, 170–176 (2019). https://doi.org/10.1038/s41557-018-0171-z
75. A. Gładysiak, P. Schouwink, S.M. Moosavi, Data-driven design and synthesis of metal- organic frameworks for wet flue gas CO_2 capture. Nature (2019). https://doi.org/10.1038/s41586-019-1798-7

76. J. Blahut, A.L. Lejeune, S. Ehrling, I. Senkovska, S. Kaskel, F.M. Wisser, G. Pintacuda, Monitoring dynamics, structure, and magnetism of switchable metal-organic frameworks via H-1-detected MAS NMR. Angew. Chemie IE. **60**(40), 21778–21783 (2021). https://doi.org/10.1002/anie.202107032
77. V. Martins, J. Xu, X. Wang, K. Chen, I. Hung, Z. Gan, C. Gervais, C. Bonhomme, S. Jiang, A. Zheng, B.E.G. Lucier, Y. Huang, Higher magnetic fields, finer MOF structural information: 17O solid-state NMR at 35.2 T. J. Am. Chem. Soc. **142**(35), 14877–14889 (2020). https://doi.org/10.1021/jacs.0c02810
78. C.M. Rice, Z.H. Davis, D. McKay, G.P.M. Bignami, R.G. Chitac, D.M. Dawson, R.E. Morris, S.E. Ashbrook, Following the unusual breathing behaviour of 17O-enriched mixed-metal (Al, Ga)-MIL-53 using NMR crystallography. Phys. Chem. Chem. Phys. **22**(26), 14514–14526 (2020). https://doi.org/10.1039/d0cp02731f
79. D. Carnevale, G. Mouchaham, S.J. Wang, M. Baudin, C. Serre, G. Bodenhausen, D. Abergel, Natural abundance oxygen-17 solid-state NMR of metal organic frameworks enhanced by dynamic nuclear polarization. Phys. Chem. Chem. Phys. **23**(3), 2245–2251 (2021). https://doi.org/10.1039/d0cp06064j
80. L. Li, I. Da Silva, D.I. Kolokolov, X. Han, J. Li, G. Smith, Y. Cheng, L.L. Daemen, C.G. Morris, H.G.W. Godfrey, N.M. Jacques, X. Zhang, P. Manuel, M.D. Frogley, C.A. Murray, A.J. Ramirez-Cuesta, G. Cinque, C.C. Tang, A.G. Stepanov, S. Yang, M. Schroder, Post-synthetic modulation of the charge distribution in a metal-organic framework for optimal binding of carbon dioxide and sulfur dioxide. Chem. Sci. **10**(5), 1472–1482 (2019). https://doi.org/10.1039/c8sc01959b
81. W.J.F. Trenholme, D.I. Kolokolov, M. Bound, S.P. Argent, J.A. Gould, J. Li, S.A. Barnett, A.J. Blake, A.G. Stepanov, E. Besley, T.L. Easun, S. Yang, M. Schröder, Selective gas uptake and rotational dynamics in a (3,24)-connected metal-organic framework material. J. Am. Chem. Soc. **143**(9), 3348–3358 (2021). https://doi.org/10.1021/jacs.0c11202
82. A. Torres-Huerta, D. Galicia-Badillo, A. Aguilar-Granda, J.T. Bryant, F.J. Uribe-Romo, B. Rodríguez-Molina, Multiple rotational rates in a guest-loaded, amphidynamic zirconia metal-organic framework. Chem. Sci. **11**(42), 11579–11583 (2020). https://doi.org/10.1039/D0SC04432F
83. I. Liepuoniute, C.M. Huynh, S. Perez-Estrada, Y.Y. Wang, S. Khan, K.N. Houk, M.A. Garcia-Garibay, Enhanced rotation by ground state destabilization in amphidynamic crystals of a dipolar 2,3-difluorophenylene rotator as established by solid state H-2 NMR and dielectric spectroscopy. J. Phys. Chem. C **124**(28), 15391–15398 (2020). https://doi.org/10.1021/acs.jpcc.0c05314
84. J. Perego, C.X. Bezuidenhout, S. Bracco, G. Prando, L. Marchio, M. Negroni, P. Carretta, P. Sozzani, A. Comotti, Benchmark mobility at a few kelvins and dynamics control by CO_2. J. Am. Chem. Soc. **143**, 13082–13090 (2021). https://doi.org/10.1021/jacs.1c03801
85. C.S. Vogelsberg, F.J. Uribe-Romo, A.S. Lipton, S. Yang, K.N. Hou, S. Brown, M.A. Garcia-Garibay, Ultrafast rotation in an amphidynamic crystalline metal organic framework. Proc. Natl. Acad. Sci. USA **114**(52), 13613–13618 (2017). https://doi.org/10.1073/pnas.1708817115
86. Y.-S. Su, E.S. Lamb, I. Liepuoniute, A. Chronister, A.L. Stanton, P. Guzman, S. Pérez Estrada, T.Y. Chang, K.N. Houk, M.A. Garcia-Garibay, S.E. Brown, Dipolar order in an amphidynamic crystalline metal-organic framework through reorienting linkers. Nat. Chem. **13**(3), 278–283 (2021). https://doi.org/10.1038/s41557-020-00618-6
87. J. Tang, Y.Y. Chu, S.H. Li, J. Xu, W.P. Xiong, Q. Wang, F. Deng, Breathing effect via solvent inclusions on the linker rotational dynamics of functionalized MIL-53. Chem. Eur. J. **27**(59), (2021). https://doi.org/10.1002/chem.202102419
88. E. Meirovitch, Z.C. Liang, J.H. Freed, Structural dynamics by nmr in the solid state: the unified MOMD perspective applied to organic frameworks with interlocked molecules. J. Phys. Chem. B **124**(29), 6225–6235 (2020). https://doi.org/10.1021/acs.jpcb.0c03687
89. P. Martinez-bulit, C.A.O. Keefe, K. Zhu, R.W. Schurko, S.J. Loeb, C.A. O'Keefe, K. Zhu, R.W. Schurko, S.J. Loeb, C.A.O. Keefe, K. Zhu, R.W. Schurko, S.J. Loeb, Solvent and steric influences on rotational dynamics in porphyrinic metal-organic frameworks with mechanically interlocked pillars. Cryst. Growth Des. **19**(10), 5679–5685 (2019)
90. G. Gholami, B.H. Wilson, K. Zhu, C.A. O'Keefe, R.W. Schurko, S.J. Loeb, Exploring the dynamics of Zr-based metal-organic frameworks containing mechanically interlocked molecular shuttles. Faraday Discuss. **225**, 358–370 (2021). https://doi.org/10.1039/d0fd00004c
91. Z.Y. Liu, Y.Y. Wang, M.A. Garcia-Garibay, Rotational dynamics of an amphidynamic zirconium metal- organic framework determined by dielectric spectroscopy. J. Phys. Chem. Lett. **12**(24), 5644–5648 (2021). https://doi.org/10.1021/acs.jpclett.1c01333

92. K. Ohazama, T. Ueda, K. Ukai, M. Ichikawa, H. Masu, H. Kajiro, H. Kanoh, Structural dynamics of an ELM-11 framework transformation accompanied with double-step CO2 gate sorption: an NMR spin relaxation study. Cryst. **10**(4), 328 (2020). https://doi.org/10.3390/CRYST10040328
93. A.J. Stirk, B.H. Wilson, C.A. O'Keefe, H. Amarne, K. Zhu, R.W. Schurko, S.J. Loeb, Applying reticular synthesis to the design of Cu-based MOFs with mechanically interlocked linkers. Nano Res. **14**(2), 417–422 (2021). https://doi.org/10.1007/s12274-020-3123-z
94. A. Saura-Sanmartin, A. Martinez-Cuezva, D. Bautista, M.R.B. Marzari, M.A.P. Martins, M. Alajarin, J. Berna, Copper-linked rotaxanes for the building of photoresponsive metal organic frameworks with controlled cargo delivery. J. Am. Chem. Soc. **142**(31), 13442–13449 (2020)

Publisher's Note Springer Nature remains neutral with regard to jurisdictional claims in published maps and institutional affiliations.